

Building Efficient Neural Networks For Brain Tumor Detection

¹Divya Shree , ²Chander Kant (Corresponding Author)

¹Assistant professor, CSE department, UIET MDU, Rohtak

²Professor, Deptt. Of Computer Sc. & Applications, K.U. Kurukshetra

¹divspanghal@gmail.com, ²ckverma@rediffmail.com

Abstract

Brain tumor detection and monitoring is essential for any indicative system, as evidenced by years of research and the steady improvement of diagnostic techniques. Accordingly, treatment planning is essential to enhancing a patient's quality of life. There is an argument that deep learning could help with the difficulties of diagnosing and treating brain tumors. In this work, we introduced a hybrid deep neural network that combines state-of-the-art image enhancement methods such as contrast stretching, histogram Equalization, and logarithmic transformation with transfer learning, similar to DenseNet169 as well as ResNet149. Work provides a deep aspect of how can we improve the accuracy and efficiency of DCNN for prediction. For data selection, we create custom data which is derived from Br35H and Fig share repository, data containing benign, malignant, and normal images (596,928,364) after enhanced. Performance analyzed different scenarios different like all three enhancement algorithms data train with each neural network and evaluate performance. Performance results show the proposed work has significant improvement with Histogram equalized data with DenseNet169 which generated accuracy of 93.29%, precision of 94%, recall of 88%, score of 93%, and loss of 20.37% which is the highest matrices over all trained neural networks in this work presented.

Keywords: Brain Tumor, Deep Learning, Dense Net, ResNet, Benign, Malignant, Contrast Stretching, Histogram Equalization, Log Transformation.

1. Introduction

A brain tumor is an abnormal, unchecked growth of cells. Some are considered "primary" because they manifest first in the brain. Those that metastasize here from elsewhere in the body are categorized as secondary. Primary brain tumors can be either malignant or benign, and they do not metastasize to other parts of the body (Zahid et al., 2022). Malignant growths arising in the brain as a secondary condition never occur in a benign form. Both can be seriously debilitating or even fatal. Growth increases intracranial pressure, which can lead to problems like edema, Due to the skull's limited volume, decreased blood flow and tissue degeneration occur (Srinivas et al., 2022).

Brain tumors are the second leading cancer killer of young people. The US Central Brain Tumor Registry predicts 64,530 new cases of primary brain and CNS tumors in 2011. This illness affects 600,000 people worldwide.

Successful therapy, as well as treatment planning, rely on an early and precise diagnosis of a brain tumor. However, only trained neuro radiologists should attempt to make a diagnosis due to the enormous variability and complexity of tumor classification in images. Recent years have seen a number of studies aimed at improving both the detection and treatment of brain tumors. The fact that MR imaging doesn't require any kind of patient-harming

manipulation is perhaps the greatest benefit of this method.

Tumors seem to be malignant cells that form when the growth of cancerous cells in any area of the body is not checked; when this happens in the brain, the outcome is a brain tumor. Computing Tomography (CT)(Tazin et al., 2021), Magnetic Resonance Imagery (MRI)(Srinivas et al., 2022), and Ultrasound are just a few examples of Medical Imaging Technology (MIT) that can be used to diagnose illness. Magnetic resonance imaging (MRI) is regarded as the best of these methods for detecting brain tumors. This happens because it is highly sensitive to local changes in tissue density while also providing specific information about the size, type, and location of individual cells. Because of the high cost associated with employing a highly trained neuroradiologist to manually examine MRI scans for signs of brain abnormalities (Sharma et al., 2022)and because of the time, it takes to do so, researchers have proposed alternative, more efficient methods of doing so, such as the use of automated procedures.

Most scientists agree that CV(Abbood, Shallal and Fadhel, 2021) can be used to automatically detect brain tumors. In the field of machine learning, CNN represents the most recent development and state-of-the-art application, and it is used for disease diagnosis using medical images, especially CT and MRI scans. Since CNN can be trained without any preprocessing or feature extraction, it has recently found widespread use in the classification and grading of medical images. For the most part, CNNs are employed to deal with raw images, with the pre-processing steps for the data being minimized or even eliminated. Typical CNN layers include an input layer, a convolution layer, a RELU layer, a fully connected layer, a classification layer, as well as an output layer(Younis et al., 2022) architecture. Both A convolutional neural network relies heavily on the convolution, which is carried out by trainable filters with the

set limits that are tuned during the training stage, and indeed the down-sampling.

After all of these problems, there is still a need to work more on research. In this work, we proposed and focused on state-of-the-art image enhancement algorithms, worked on data with three classes, and utilized an advanced deep neural network DCNN(Sharma et al., 2022) that was based on transfer learning. The primary objective of this work was to improve the feature extraction efficiency of CNN model using existing image enhancement algorithms with fewer data.

2. Related Work

The classification of brain tumors is an important and active area of research in the modern era. Quite a few methods, including deep learning-based, best features selection-based, and a great number of others, have been developed recently(Younis et al., 2022)(Rajesh Babu et al., 2019).Most research on (Zahid et al., 2022) has focused on FLAIR, T1, T2, and T1CE tumor classification using deep learning. We normalized the dataset to transfer-learn from ResNet101. This tweaks the ResNet101 brain tumor classification model. This method creates duplicate features. These redundant features reduce accuracy and increase CPU usage. Using deferential evaluation but also particle swarm optimization, we find optimal features. Optimal feature vectors have been serially fused to create a single-fused vector. The final effective feature vector is derived from this fused vector using PCA. This optimized feature vector helps classify tumors. Multiple stages of performance are analyzed. The suggested methodology sped up medium neural network classification time by 25.5x with 94.4% accuracy. These results show a significant reduction in computational cost while maintaining accuracy.

In the 2021s, (Díaz-Pernas et al., 2021) was considered aim for multiscale DCN-based automatic segmentation and classification of brain tumors. In contrast to competing proposals, ours involves processing input

images on three distinct spatial scales. This system is an analog to the HVS. Without first removing skull or spinal column parts, the proposed neural model can analyze MRI images of meningioma, glioma, and pituitary tumors in sagittal, coronal, and axial views. On a publicly available MRI image dataset consisting of 3064 slices from 233 patients, we evaluate our method alongside traditional machine learning and deep learning approaches. When compared to other approaches using the same database, ours was more accurate at classifying tumors.

(Vankdothu and Hameed, 2022) Has attracted considerable attention form of automated detection and classification system. The method includes Segmentation, feature extraction, and classification from magnetic resonance imaging (MRI) datasets. Preprocessing the MRI images uses an adaptive filter to get rid of the noise. The images are segmented with IKMC and features are extracted with GLCM. To identify gliomas, meningiomas, benign lesions, and malignant tumors in the pituitary gland, we trained a deep learning model on MRI scans. Classification was performed using RCNNs (RCNN). Input brain images are better classified by the proposed method. These tests made use of MRI images from Kaggle's 394 testing sets and 2870 training sets. The findings demonstrate that the proposed approach is superior to the state-of-the-art. The article concludes with a comparison of RCNN to BP, U-Net, and RCNN. The proposed classifier classified brain tumors from MRI images with 95.1% accuracy.

Most recently research on (Alnowami et al., 2022) has focused on artificial neural networks to automate brain tumor detection in MRI tests. A total of 4314 MRI scans were used in this investigation. Normal brain tissue, glioma tissue, meningioma tissue, and pituitary tumor tissue are the four categories present in the data. Several preprocessing steps are applied to raw data before the modeling process begins, and the effectiveness of each is assessed. DenseNet was trained with data from

three different sources. Improvements in classification can be achieved by increasing contrast and normalizing intensities in the MRI image. Preprocessing was found to have a positive effect on the training convergence of DenseNet. After subjecting the proposed model to ten rounds of cross-validation, it was found to have a 96.52% accuracy rate, a 98.5% sensitivity rate, and an 82.1% specificity rate. Finally, we draw the conclusion that preprocessing steps benefit the performance of automated deep learning systems for tumor segmentation.

Brain tumors, a common and aggressive disease, shorten lives. Treatment planning improves a patient's quality of life. CT, MRI, and ultrasound are used to evaluate prostate, breast, lung, and brain tumors. MRIs are used to detect brain tumors. Massive amounts of MRI data prevent manual tumor vs. non-tumor classification. With few images, it lacks quantitative precision. To avoid human mortality, (Abbood, Shallal and Fadhel, 2021) suggested an automated classification system. Space and structural variability make automatic brain tumor categorization difficult. This comparative study classifies brain tumors using AlexNet, VGG16, GoogleNet, and RestNet50. RestNet50 has the highest accuracy with 95.8%, while AlexNet is the fastest with 1.2 seconds. AlexNet (the fastest model) has a real-time GPU processing time of 8.3 msec.

3. Proposed Methodology

Herein, we introduce a fully automated method for brain tumor categorizing in this study. This research analyses the relationships between 2 types of tumors that can develop in the brain. These are the procedures for the following that are being implemented:

- a. Preprocessing is applied to enhance the image dataset, normalize images, and applied an image data generator.
- b. To enhance the images applied three state-of-art algorithms (Qi et al., 2022) likewise contrast stretching, histogram

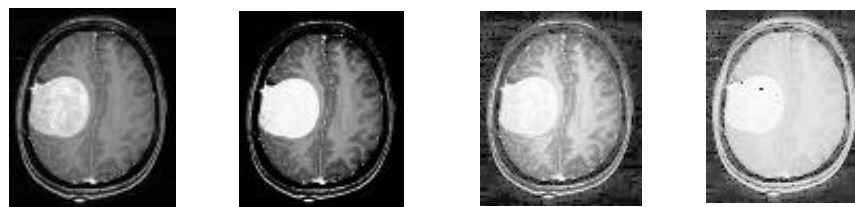
Equalization, and logarithmic transformation.

- c. The DenseNet169(Zhong et al., 2020), ResNet152(Liang, 2020)pre-trained models were implemented and fine-tuned using the transfer learning method used for prediction and classification.

3.1 Dataset Collection and Preprocessing

During the course of this research, we compiled a unique dataset using data from two separate sources, namely Br35H(Kang, Ullah and Gwak, 2021) and figshare(brain tumor dataset, no date). Br35H contains images that are classified as either positive or negative. Images that are classified as negative have no class. Pituitary tumour (708 slices), glioma (1,426 slices), and meningioma (708 slices) are the three different types of brain tumours that are represented in the brain tumour dataset on figshare, which contains T1-weighted contrast-enhanced images. The dataset was collected from 233 patients (930 slices). When it comes to making a custom data selection, we take into consideration three different types of images: benign (149), malignant (232), and normal (91). Figure 1(a),2(a),3(a) shows the few example of original data set images before process in which class as follows Benign, Malignant, and Normal.

For preprocessing and image enhancement we perform three image



(a) (b)(c)(d)

Fig 1.Enhanced Benign Tumor images using Contrast Stretching (b), Histogram Equalization (c), and Logarithmic Transformation (d) and Original image (a).

b.Histogram Equalization

This technique improves the global contrast of many images, especially those with few

enhancement algorithms called contrast stretching, histogram Equalization, and logarithmic transformation. Processing steps and information of all preprocessing images as follows:

a. Contrast Stretching

It is necessary to first specify the upper and lower pixel value limits over which the image is to be normalized in order for the stretching process to even begin. Only then can the image be stretched(Dr. Faten A. Dawood, 2018). Most of the time, these limits will simply consist of the minimum and maximum pixel values that are permitted by the image type in question. For grayscale images with 8 bits of resolution, for instance, the lower limit might be 0 and the upper limit might be 255. Let's refer to the lower limit as **a** and the upper limit as **b** respectively(T C, S and N, 2011). The most basic form of image normalization begins by scanning the image in order to locate the pixel values that are currently at their lowest and highest extremes. We'll refer to these as **c** and **d**. Then the following function is applied to each pixel **P** in order to scale them:

$$P_{out} = (P_{in} - c) \frac{(b-a)}{(d-c)} + a \quad (1)$$

The values that are less than 0 are reset to 0, and the values that are between 0 and 255 are reset to 255(Point Operations - Contrast Stretching, no date).

intensity values. This change allows a more uniform application of histogram intensities. Low-contrast areas can improve. Histogram

equalization('Histogram Equalization', 2009) spreads out image contrast-reducing dense intensity values. Back estimation (or "project") of a histogram image refers to the application of the modified histogram to the main image as a look-up table for pixel brightness values. The function uses the values of pixels in each feedback group taken from the exact position in all individual images to determine the location of the histogram bin in the output image. The value of each pixel in the output image is the probability that the input pixel group to which it corresponds is a part of the object whose histogram is being used (Senthilkumaran and Thimmiraja, 2014). To enhance images using histogram equalization `cv2.equalizeHist`, convert all images into BGR to YUV color format then equalize Y channel of using python list slicing process convert image into RGB using YUV to BGR function. Typically, a red, green, and blue (RGB) source is used to generate an Y'UV signal (Umer et al., 2020). Y', a luminance value, is calculated by adding the average of the RGB values. Discovering the ratios of Y' to B and R allows us to calculate U and V. From the BT.470 System M primaries as well as white point using SMPTE RP 177, the PAL standard defines the following constants (NTSC used YIQ, which is further rotated) (these same predictor variables, called matrix coefficients, were later used in BT.601,

though this uses 1/2 instead of 0.436 as well as 0.615).

$$W_R = 0.299, W_G = 1 - W_R - W_b = 0.587, W_B = 0.144, U_{\max} = 0.436, V_{\max} = 0.615.$$

Using the R'G'B' color space, PAL signals can be converted to the Y'UV range.

$$Y' = W_R R' + W_G G' + W_b B' = 0.299R' + 0.587G' + 0.114B' \quad (2)$$

$$U = U_{\max} \frac{B' - Y'}{1 - W_B} \approx 0.492(B' - Y') \quad (3)$$

$$V = V_{\max} \frac{R' - Y'}{1 - W_R} \approx 0.877(R' - Y') \quad (4)$$

$$S_k = T(r_k) = (L - 1) \sum_{j=0}^k p_r(r_j) \quad (5)$$

Where "s" and "r" represent the pixel intensities that are sent out and taken in, respectively. "L" denotes the highest possible intensity level (for n-bit images $L = 2^n$). The following equation provides a rough estimate of the frequency with which pixel intensity levels r_i , r_j and n_j appear in:

$$p_r(r_j) = \frac{n_j}{MN} \quad (6)$$

Where MN is the total number of pixels and n_j is the number with intensity r_j . 2, 3, 4 relate to RGB to YUV conversion, and 5 and 6 to histogram equalization. Invert 2,3,4 for RGB image (Kalyani and Chakraborty, 2020).

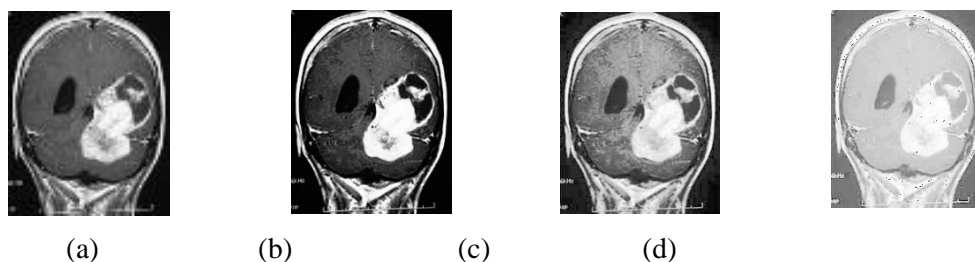


Fig 2. Enhanced Malignant Tumor images using Contrast Stretching (b), Histogram Equalization (c), and Logarithmic Transformation (d) and Original image (a).

C. Logarithmic Transformation

Log transformation refers to a method of data transformation in which each x-valued variable is replaced by its logarithm (x). The logarithmic (Tezcan et al., 2019) basis used in the analysis is typically determined by the

objectives of the statistical modelling. For the natural history record, type ln. To improve the reliability of statistical analysis results when dealing with data that does not conform to the bell curve, log transformation can be used. In other words, the log transformation reduces or

gets rid of the distortion in our original data. A log-normal distribution, or one very close to one, must exist in the original data. When this is not the case, the log transformation will fail (geeks, 2020). Here is the logarithmic transformation (Attar et al., 2018) formula:

$$s = c \log(r + 1) \quad (7)$$

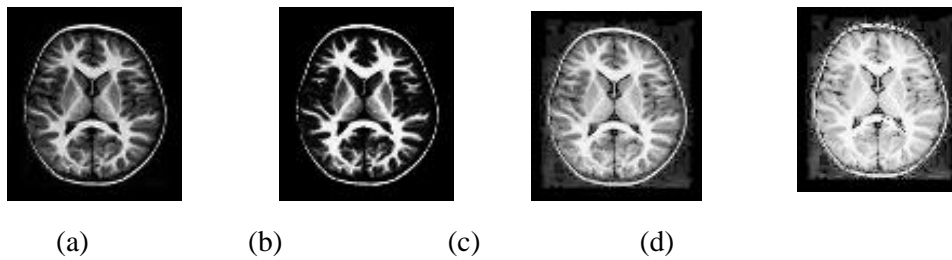


Fig 3. Enhanced Malignant Tumor images using Contrast Stretching (b), Histogram Equalization (c), and Logarithmic Transformation (d) and Original image (a).

3.2 Deep Neural Network Model

Recent advances in image classification have been made by deep neural networks (Lin et al., 2018; Wahlang et al., 2022). Deep models combine low-, mid-, and high-level features. We use DenseNet169, ResNet152 to extract features and classification. A Dense Net ('DenseNet Convolutional Neural Networks ...ID-19 Using CT Image_Enhanced Reader.pdf', no date) which uses dense connections between layers, is a subclass of convolutional neural networks. For feed-forward to function, each layer must take in data from lower layers and send out feature maps to higher layers. The information bottleneck is alleviated thanks to Huang's dense blocks because they are the first to introduce dense intercommunication, which means that each layer receives a signal from all of the layers below it through a single channel. As a means of enhancing feature reuse and extraction, Dense Net makes use of identity mappings, deep supervision, decreased feature

Pixel values for the output and input images are s and r , respectively, and c is a constant. With an input image's pixel intensity set to o , and $\log(o)$ equaling infinity, we must multiply each pixel value by 1. This results in the minimum number being raised by one to ensure there is at least one (Ker et al., 2017).

redundancy, and diversified depth. Out of DenseNet121, 169, 209, and 264, the accuracy of DenseNet121 is highest (Tao et al., 2020). Number of layers equals 121, where 5 is the convolution as well as pooling layer, 3 is the transition layer (6,12,24), 1 is the classification layer (16), and 2 are the dense block (1*1 and 3*3 conv). With the completion of CNN's architecture, the network achieved groundbreaking results and ultimately won the ILSVRC classification competition in 2015 (Hasan et al., 2021). ResNet (Kawauchi et al., 2020) reduces the vanishing gradient problem (which occurs when an error gradient is back-propagated and gradually decreases) (training deep networks incorporates backpropagation of error gradient which gets reduced as it passes in the backward direction). They used skip connections to get around the infinite gradient (Fig. 4). Image classification is a strong suit of ResNet and its variants. DenseNet169 was selected because it effectively learned representations of images (Zhou et al., 2021).

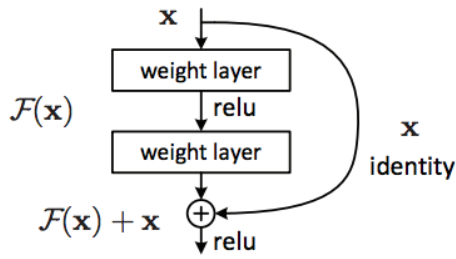


Fig 4. Residual Learning: Block of a Layer

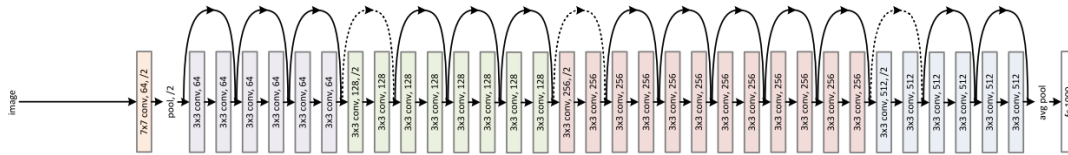


Fig 5. Architecture of ResNet.

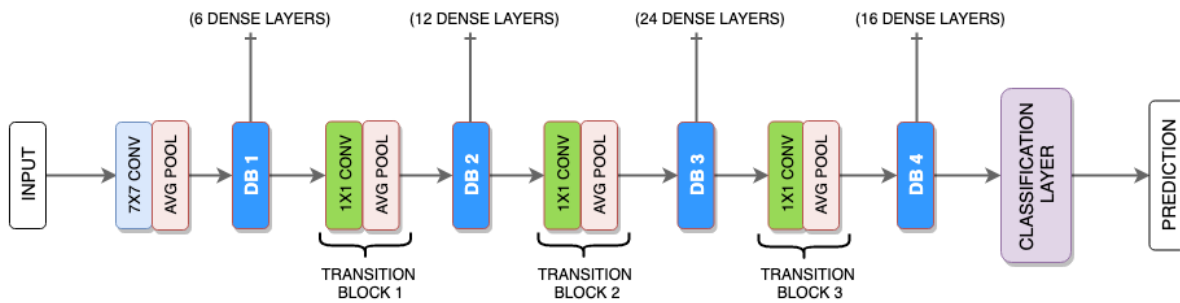


Fig 6- DenseNet architecture.

3.3 Transfer Learning

Transfer learning (TL)(Valverde et al., 2021) is indeed a research form of machine learning (ML) that remembers what it's learned from one problem and uses it to solve another, unrelated one; for instance, recognizing cars may help with recognizing trucks(Kim et al., 2022). While there is little in the way of direct application between this and the vast body of literature on the transfer of learning in psychology, there are some interesting connections to be made. From a practical standpoint, a supervised learning agent's sample efficiency can be greatly improved by

reusing or transferring data from the previous knowledge for the learning of new tasks. In 1976, Stevo Bozinovski(Bozinovski, 2020)jointly published research on the direct effects of transfer learning on neural network-based instruction led by Ante Fulgosi. In the paper, we will present a model of transfer learning that is both mathematical and geometric in nature. In order to train a neural network, transfer learning was used 1981, with data consisting of images of computer concourse letters. Experimental evidence supported both the positive and negative aspects of transfer learning.

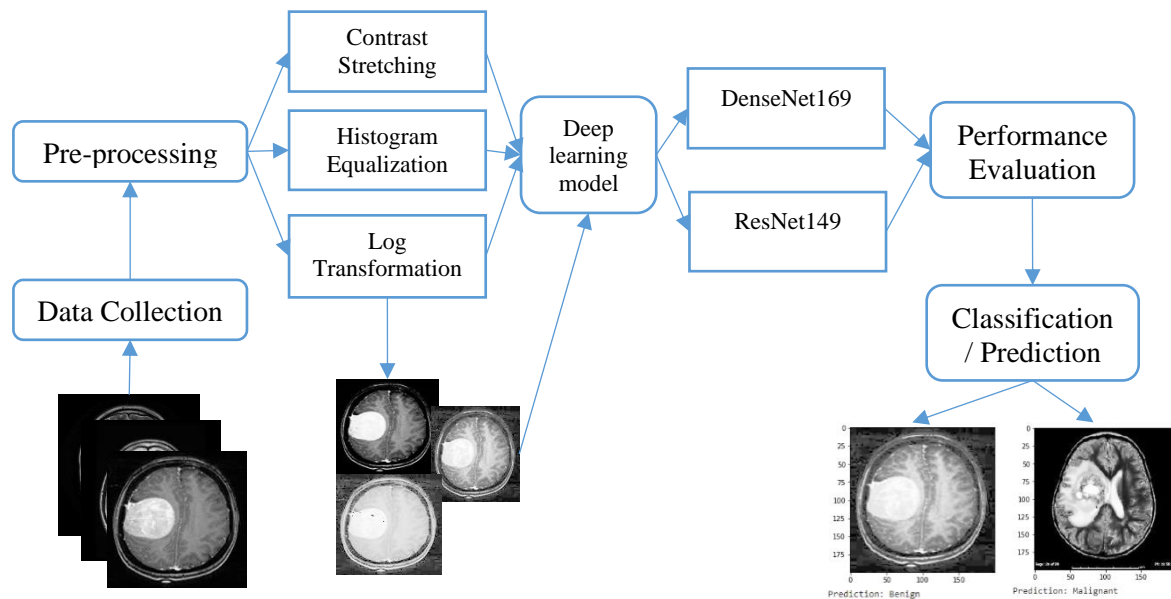


Fig 6. Flowchart of proposed methodology for Brain tumor classification.

In table 1, rows represent tumor type and columns represent enhanced algorithms with image distribution.

Table 1 Custom Dataset Description.

Tumor Type	Original Data	Contrast Enhanced	Histogram Equalized	Log Transformed	Total Images
Benign	149	149	149	149	596
Malignant	232	232	232	232	928
Normal	91	91	91	91	364

3.4 Training Procedure

Figure 6 represent the complete process of processing and training. After enhancing images using data passes to neural network to train and learn features of image. The following is the procedure of figure 6 explain below.

- Generate dataset form Br35h and figshare, create Benign, Malignant and Normal images.
- Enhance these images using contrast stretching, histogram Equalization, and logarithmic transformation.
- Divide data in to ratio of 80% for training and 20% for Testing.
- Implement Resnet149 and DenseNet169 with custom 2DCNN CNN layers.
- Train models on training dataset and calculate accuracy and loss.

- Evaluate model on test data, plot accuracy, loss and confusion matrix of each model with distinct enhanced data of images.
- Finally perform classification and prediction.

4. Results and Discussion

This portion covers the in-depth discussion of numerical results, we obtained at the training and testing time of the neural network.

Dataset we used is custom dataset, it created form Br35H and figshare using convert .mat format of the file into .jpg which contain label as well with data. To define classes of three segment we select only Benign, Malignant and Normal (no tumor). Dataset based on MRI images with different aspect ratio or height and width of images. The Benign original data images contain (149), malignant

contain 232 images and normal images contain 91 images. After done image enhancement task using contrast stretching, histogram Equalization, and logarithmic transformation the total image count of each class is (596,928,364).

In preprocessing part we done three major steps like image enhancement, rescaling, resizing and normalization by division of each pixel with 255 and finally applied image data generator for generate more images it perform following operations like rotation with 360,180 degree, width and height shift with 20%, zooming with 20%, horizontal and vertical flip. After preprocessing convert all images into numpy array to train the neural network. We computed this generated data set on transfer

learning models like Resnet149(Liang, 2020; Sarwinda et al., 2021) andDenseNet169 with custom layers like Conv2D(He et al., 2016), Global Average Pooling Batch normalization, and Dropout layer with 50 %.To Activate and fire neurons we allied the Relu activation function, for classification use Softmax(Nwankpa et al., 2018) because this model contains 3 classes so final output layer contain 3 neutrons.

For optimization we used Adam optimizer(Yaqub et al., 2020) with following hyper-parameters like learning rate 0.002 with incremental, beta 1 and 2 with 0.9 and 0.999, epsilon 10 %, and decay 0. To compilation neural network use loss calculation function as categorical cross entropy andmetricsaccuracy.

Table 2.Hyper parameters summary.

Model	Sequential
Transfer Learning Model	ResNet149, DenseNet169
Type	Pre Trained
Epochs	100
Optimizer	Adam
Loss	Categorical cross entropy

This section contains information about the performance evaluation of each model on a different image-enhanced dataset.

Table 3. Performance Evaluation of Models on Contrast Stretched data.

Model	Accuracy	Precision	Recall	F-score	Loss
DenseNet169	90.62%	95%	92%	90%	31.19%
ResNet149	75.08%	79%	84%	85%	65.00%

Table 4. Performance Evaluation of Models on Histogram Equalizeddata.

Model	Accuracy	Precision	Recall	F-score	Loss
DenseNet169	93.29 %	94%	88%	93%	20.37%
ResNet149	71.88%	86%	81%	87%	34.39%

Table 5. Performance Evaluation of Models on Log Transformed data.

Model	Accuracy	Precision	Recall	F-score	Loss
-------	----------	-----------	--------	---------	------

DenseNet169	86.90%	93%	91%	94%	37.96%
ResNet149	60.70%	69%	71%	85%	100.23%

The results of our calculations for the five most important performance parameters are presented in table 3, and they are as follows: accuracy, precision, recall, f score, and loss. In comparison, the Resnet149 model only

produced an accuracy of 75.08% when given the contrast stretched image dataset. DenseNet169 performed admirably, achieving 90.62% accuracy with the dataset.

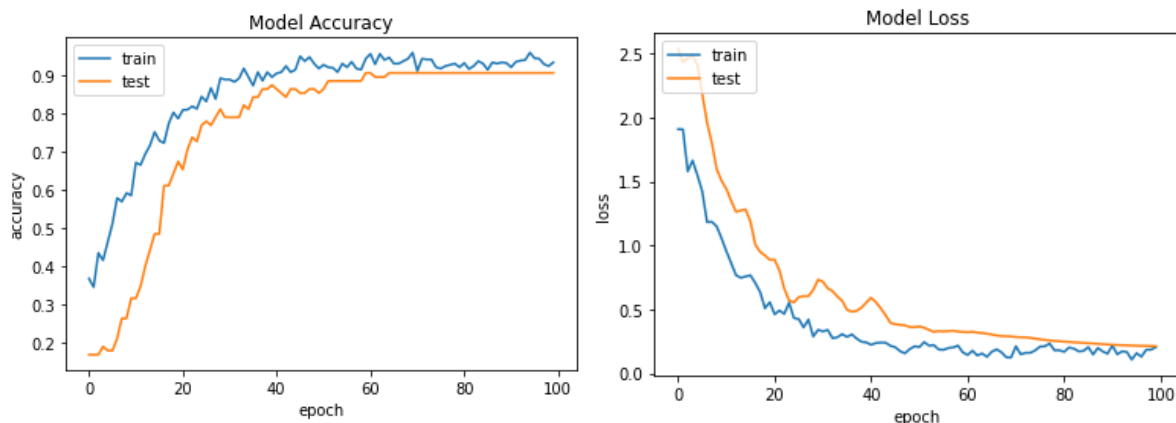


Fig 6. Accuracy and loss graph of DenseNet169.

In a similar fashion, the overall performance of Densenet169 was better in terms of all matrices, and there was less loss. In a similar vein, we are able to observe in tables 4 and 5 that Densenet169 performs quite admirably. When we take into account the overall performance of all three tables, we find that Densenet169 achieves a maximum of 93.26% when using Histogram Equalized data and a minimum of 86.90% when using Log Transformed data. In the case of Resnet, it performed the best with an accuracy of 75.08%, which was the highest possible score for Resnet149 in terms of all enhanced images; however, the worst-case scenario involved Log Transformed data.

The results of our experiments indicate that the recommended networks are accurate because they are able to achieve astonishingly good results in Brain Tumour Detection detection tasks with the accuracies they were trained with. Figure 6 illustrates both the model accuracy graph of outcomes and the model loss graph of outcomes after epochs. Both graphs are displayed in the figure. The confusion matrix that was performed on the test data can be seen in Figure 7. The confusion matrix compares the actual data to the data that was predicted.

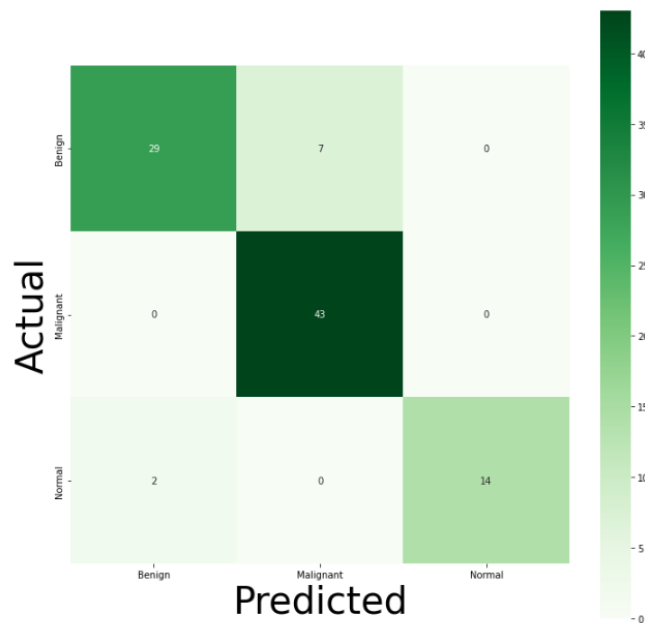


Fig 7. Confusion matrix of DenseNet169 on test data.



Fig 8. Predicted images of Benign (a) and Malignant (b) classes.

Finally we compare DenseNet169 and ResNet149 individually for each type of enhanced image dataset, after all we find that the DenseNet169 performed well on all type of data which is generated using custom process and give higher accuracy over low amount of data set, in this phase we didn't see any under sampling at the time of training and testing with DenseNet169 model, as we can see in figure 7 classes which is belong to Benign, malignant and normal images predict well in the same manner figure 8 represent the final neural network predicted output with label of Benign and malignant classes.

5. Conclusion

In this work, we introduced a fully automated classification as well as prediction of Brain

Tumor classes such as Malignant and Benign. The methodology is based on Transfer learning and state-of-the-art image enhancement algorithms, including the DenseNet169 and ResNet149 models are hybridized with custom layers. In this way, we were able to distinguish between benign and malignant Brain Tumors. The model was evaluated using three different enhancement algorithms' data, all of which process MRI Brain tumor images. The dataset was designed using a custom process, and the images came from Br35H and Figshare respectively. Python was used for the ImageDataGenerator function of the Open CV library, which was used for data augmentation. Both by itself and in comparison to Resnet149, our model achieved the highest classification accuracy. Accuracy-wise, we came up with a

value of 93.29% for DenseNet169 when using Histogram Equalized data. The diagnosis of brain tumors and other imaging-related medical issues are both possible utilizing our technique. Developing an FCN architecture for MRI image classification and comparing it to the proposed model are both potential aspects of the work that could be done. On top of that, we intend to evaluate the performance of the multiscale convolutional neural networks using satellite imagery.

References

1. Abbood, A. A., Shallal, Q. M. and Fadhel, M. A. (2021) 'Automated brain tumor classification using various deep learning models: A comparative study', *Indonesian Journal of Electrical Engineering and Computer Science*, 22(1), pp. 252–259. doi: 10.11591/ijeecs.v22.i1.pp252-259.
2. Alnowami, M. et al. (2022) 'MR image normalization dilemma and the accuracy of brain tumor classification model', *Journal of Radiation Research and Applied Sciences*, 15(3), pp. 33–39. doi: 10.1016/j.jrras.2022.05.014.
3. Attar, T. et al. (2018) 'Parametric Optimization of Logarithmic Transformation using GWO for Enhancement and Denoising of MRI Images', 3rd International Conference and Workshops on Recent Advances and Innovations in Engineering, ICRAIE 2018, pp. 1–7. doi: 10.1109/ICRAIE.2018.8710393.
4. Bozinovski, S. (2020) 'Reminder of the first paper on transfer learning in neural networks, 1976', *Informatica (Slovenia)*, 44(3), pp. 291–302. doi: 10.31449/INF.V44I3.2828.
5. brain tumor dataset (no date). Available at: https://figshare.com/articles/dataset/brain_tumor_dataset/1512427 (Accessed: 1 October 2022).
6. 'DenseNet Convolutional Neural Networks ...ID-19 Using CT Image _ Enhanced Reader.pdf' (no date).
7. Díaz-Pernas, F. J. et al. (2021) 'A deep learning approach for brain tumor classification and segmentation using a multiscale convolutional neural network', *Healthcare (Switzerland)*, 9(2). doi: 10.3390/healthcare9020153.
8. Dr. Faten A. Dawood (2018) 'The Importance of Contrast Enhancement in Medical Images Analysis and Diagnosis', *International Journal of Engineering Research and*, V7(12), pp. 21–24. doi: 10.17577/ijertv7is120006.
9. geeks (2020) Log transformation of an image using Python and OpenCV, Geeks for Geeks.
10. Hasan, N. et al. (2021) 'DenseNet Convolutional Neural Networks Application for Predicting COVID-19 Using CT Image', *SN Computer Science*, 2(5), pp. 1–11. doi: 10.1007/s42979-021-00782-7.
11. He, K. et al. (2016) 'Deep residual learning for image recognition', in *Proceedings of the IEEE Computer Society Conference on Computer Vision and Pattern Recognition*. doi: 10.1109/CVPR.2016.90.
12. 'Histogram Equalization' (2009) *Encyclopedia of Biometrics*, pp. 707–707. doi: 10.1007/978-0-387-73003-5_629.
13. Kalyani, J. and Chakraborty, M. (2020) 'Contrast Enhancement of MRI Images using Histogram Equalization Techniques', 2020 International Conference on Computer, Electrical and Communication Engineering, ICCECE 2020, pp. 2–6. doi: 10.1109/ICCECE48148.2020.9223088.
14. Kang, J., Ullah, Z. and Gwak, J. (2021) 'Mri-based brain tumor classification using ensemble of deep features and machine learning classifiers', *Sensors*, 21(6), pp. 1–21. doi:

- 10.3390/s21062222.
15. Kawauchi, K. et al. (2020) 'A convolutional neural network-based system to classify patients using FDG PET/CT examinations', *BMC Cancer*, 20(1), pp. 1–10. doi: 10.1186/s12885-020-6694-x.
 16. Ker, J. et al. (2017) 'Deep Learning Applications in Medical Image Analysis', *IEEE Access*, 6, pp. 9375–9379. doi: 10.1109/ACCESS.2017.2788044.
 17. Kim, H. E. et al. (2022) 'Transfer learning for medical image classification: a literature review', *BMC Medical Imaging*, 22(1), pp. 1–13. doi: 10.1186/s12880-022-00793-7.
 18. Liang, J. (2020) 'Image classification based on RESNET', *Journal of Physics: Conference Series*, 1634(1), pp. 1–7. doi: 10.1088/1742-6596/1634/1/012110.
 19. Lin, W. et al. (2018) 'Convolutional neural networks-based MRI image analysis for the Alzheimer's disease prediction from mild cognitive impairment', *Frontiers in Neuroscience*, 12(NOV), pp. 1–13. doi: 10.3389/fnins.2018.00777.
 20. Nwankpa, C. et al. (2018) 'Activation Functions: Comparison of trends in Practice and Research for Deep Learning', pp. 1–20. Available at: <http://arxiv.org/abs/1811.03378>.
 21. Point Operations - Contrast Stretching (no date). Available at: <https://homepages.inf.ed.ac.uk/rbf/HIPR2/stretch.htm> (Accessed: 1 October 2022).
 22. Qi, Y. et al. (2022) 'A Comprehensive Overview of Image Enhancement Techniques', *Archives of Computational Methods in Engineering*, 29(1), pp. 583–607. doi: 10.1007/s11831-021-09587-6.
 23. Rajesh Babu, K. et al. (2019) 'Comparative analysis of brain tumor detection using deep learning methods', *International Journal of Scientific and Technology Research*, 8(12), pp. 250–254.
 24. Sarwinda, D. et al. (2021) 'Deep Learning in Image Classification using Residual Network (ResNet) Variants for Detection of Colorectal Cancer', *Procedia Computer Science*, 179(2019), pp. 423–431. doi: 10.1016/j.procs.2021.01.025.
 25. Senthilkumaran, N. and Thimmiaraja, J. (2014) 'Histogram equalization for image enhancement using MRI brain images', *Proceedings - 2014 World Congress on Computing and Communication Technologies, WCCCT 2014*, pp. 80–83. doi: 10.1109/WCCCT.2014.45.
 26. Sharma, S. et al. (2022) 'Deep Learning Model for Automatic Classification and Prediction of Brain Tumor', *Journal of Sensors*, 2022. doi: 10.1155/2022/3065656.
 27. Srinivas, C. et al. (2022) 'Brain Tumor Classification Using MRI Images', 2022.
 28. T C, R. K., S, A. P. and N, K. (2011) 'Fuzzy Based Contrast Stretching for Medical Image Enhancement', *ICTACT Journal on Soft Computing*, 2(1), pp. 233–236. doi: 10.21917/ijsc.2011.0036.
 29. Tao, Z. et al. (2020) 'NSCR-Based DenseNet for Lung Tumor Recognition Using Chest CT Image', *BioMed Research International*, 2020. doi: 10.1155/2020/6636321.
 30. Tazin, T. et al. (2021) 'A Robust and Novel Approach for Brain Tumor Classification Using Convolutional Neural Network', *Computational Intelligence and Neuroscience*, 2021. doi: 10.1155/2021/2392395.
 31. Tezcan, K. C. et al. (2019) 'MR Image Reconstruction Using Deep Density Priors', *IEEE Transactions on Medical Imaging*, 38(7), pp. 1633–1642. doi: 10.1109/TMI.2018.2887072.

32. Umer, M. et al. (2020) 'A novel stacked CNN for malarial parasite detection in thin blood smear images', *IEEE Access*, 8, pp. 93782–93792. doi: 10.1109/ACCESS.2020.2994810.
33. Valverde, J. M. et al. (2021) 'Transfer learning in magnetic resonance brain imaging: A systematic review', *Journal of Imaging*, 7(4), pp. 1–21. doi: 10.3390/jimaging7040066.
34. Vankdothu, R. and Hameed, M. A. (2022) 'Brain tumor MRI images identification and classification based on the recurrent convolutional neural network', *Measurement: Sensors*, 24(August), p. 100412. doi: 10.1016/j.measen.2022.100412.
35. Wahlang, I. et al. (2022) 'Brain Magnetic Resonance Imaging Classification Using Deep Learning Architectures with Gender and Age', *Sensors*, 22(5), pp. 1–20. doi: 10.3390/s22051766.
36. Yaqub, M. et al. (2020) 'State-of-the-art CNN optimizer for brain tumor segmentation in magnetic resonance images', *Brain Sciences*, 10(7), pp. 1–19. doi: 10.3390/brainsci10070427.
37. Younis, A. et al. (2022) 'Brain Tumor Analysis Using Deep Learning and VGG-16 Ensembling Learning Approaches', *Applied Sciences*, 12(14), p. 7282. doi: 10.3390/app12147282.
38. Zahid, U. et al. (2022) 'BrainNet: Optimal Deep Learning Feature Fusion for Brain Tumor Classification', *Computational Intelligence and Neuroscience*, 2022. doi: 10.1155/2022/1465173.
39. Zhong, Z. et al. (2020) 'Cancer image classification based on DenseNet model', *Journal of Physics: Conference Series*, 1651(1). doi: 10.1088/1742-6596/1651/1/012143.
40. Zhou, C. et al. (2021) 'COVID-19 Detection based on Image Regrouping and ResNet-SVM using Chest X-ray Images', *IEEE Access*, 9. doi: 10.1109/ACCESS.2021.3086229.
- 41.